

Biphoton in a Dispersive Medium

Alejandra Valencia, Maria V. Chekhova*, Alexei Trifonov†, and Yanhua Shih

Department of Physics, University of Maryland, Baltimore County, Baltimore, Maryland 21250

Abstract

We report an experimental study of group-velocity dispersion effect on an entangled two-photon wavepacket, generated via spontaneous parametric down-conversion and propagating through a dispersive medium. Even in the case of using CW laser beam for pump, the biphoton wavepacket and the second-order correlation function spread significantly. The study and understanding of this phenomenon is of great importance for quantum information applications, such as quantum communication and distant clock synchronization.

PACS Number: 42.50.-p, 42.50.Dv, 03.65.Ta

arXiv:quant-ph/0407201v1 26 Jul 2004

Entangled two-photon light has been proved to be useful in quantum metrology [1] and quantum communications [2]. New applications have been recently proposed, such as quantum computing, quantum information processing, and quantum lithography [3]. In all applications, the crucial feature is the measurement of the correlation of the two-photon entangled state. In many cases, the spreading of the biphoton wavepacket and the second-order Glauber correlation function [4] becomes a critical issue, especially for these applications in which the precise timing information is essential, such as synchronization of distant clocks.

Consider a very simple experiment. A pair of entangled photons is generated from spontaneous parametric down-conversion (SPDC) [5] and propagates through a dispersive medium. The dispersive medium could be in one path or both paths. Two single-photon counting detectors are used for the detection of the signal and the idler photons, respectively. In most of the two-photon interferometric experiments, coincidence counting rate is the only necessary measured quantity:

$$R_c \sim \int_0^T dt_1 dt_2 S(t_1 - t_2 - t_0) G^{(2)}(t_1, r_1; t_2, r_2), \quad (1)$$

where $G^{(2)}(t_1, r_1; t_2, r_2)$ is the second-order Glauber correlation function [4], $S(t_1 - t_2 - t_0)$ the coincidence window function, which is usually a rectangular function centered at t_0 , T the data collection time for the coincidence measurement, t_i the detection time of the i -th detector and r_i the optical path to the i -th detector. The second-order Glauber correlation function is defined as

$$G^{(2)}(t_1, r_1; t_2, r_2) = \langle E^{(-)}(t_1, r_1) E^{(-)}(t_2, r_2) E^{(+)}(t_2, r_2) E^{(+)}(t_1, r_1) \rangle, \quad (2)$$

where $E^{(-)}$ and $E^{(+)}$ are the negative-frequency and the positive-frequency field operators and ensemble averaging is done over the quantum state. In the stationary case, $G^{(2)}$ depends only on $t_1 - t_2$. In the case of two-photon state generated via SPDC, $G^{(2)}$ can be represented as the square modulo of the two-photon wave function, or biphoton,

$$\psi(t_1, r_1; t_2, r_2) \equiv \langle 0 | E^{(+)}(t_2, r_2) E^{(+)}(t_1, r_1) | \Psi \rangle, \quad (3)$$

where $\langle 0|$ denotes the vacuum state and $|\Psi\rangle$ the two-photon state of SPDC [6]. It is necessary to point out that in most of the two-photon interferometry-type measurements, in which the coincidence time window is much greater than the width of $G^{(2)}$, the temporal broadening information of the biphoton and the $G^{(2)}$ function is lost. To measure the temporal correlation function with or without broadening, one needs to measure $G^{(2)}(t_1, r_1; t_2, r_2)$, but not the time integral of $G^{(2)}(t_1, r_1; t_2, r_2)$. In the low counting rate cases, a TAC (Time-to-Amplitude-Converter) - MCA (Multi-Channel-Analyzer) system can be used to observe the shape of $G^{(2)}$, which contains the group-velocity broadening information of a biphoton. Photocurrent pulses from the first and second detectors are sent, respectively, to the “start” and “stop” inputs of a time-to-amplitude converter (TAC), where the time differences between “start” and “stop” are converted linearly to different amplitudes of the output pulses. The amplitudes of the output pulses of the TAC are analyzed by means of a multi-channel analyzer (MCA). The time resolution of the “start-stop” method is mainly determined by the resolution of the detectors, usually in the order of a few hundreds of picoseconds. The shape of $G^{(2)}$ for two-photon light emitted via SPDC can be easily calculated using Eq. (2), where ensemble averaging should be done over the state generated in SPDC,

$$|\Psi\rangle = |\text{vac}\rangle + c \int_{-\infty}^{\infty} d\Omega F(\Omega) a_i^\dagger\left(\frac{\omega_p}{2} - \Omega\right) a_s^\dagger\left(\frac{\omega_p}{2} + \Omega\right) |\text{vac}\rangle. \quad (4)$$

Here the indices s and i denote the signal and idler photons, respectively; ω_p is the pump frequency, and $\Omega \equiv \omega_s - \omega_p/2 = \omega_p/2 - \omega_i$. The coefficient c depends on the pump amplitude and the quadratic susceptibility. We consider the case of cw pump and, for simplicity, collinear frequency-degenerate phase matching. The spectral amplitude, $F(\Omega)$, provides all information about the correlation properties of two-photon light. The spectrum of signal-idler radiation is $S(\Omega) = |F(\Omega)|^2$. Even if a dispersive medium of length z_s (z_i) is included in the propagation path of the signal (idler) photon, the first-order correlation function $G^{(1)}$ of the signal (idler) radiation is given by the Fourier transform of the spectrum only,

$$G^{(1)}(\tau) \sim \int_{-\infty}^{\infty} d\Omega |F(\Omega)|^2 \cos(\Omega\tau), \quad (5)$$

where $\tau \equiv [t_2 - (z_{s,i}/u_{s,i} + r_2/c)] - [t_1 - (z_{s,i}/u_{s,i} + r_1/c)]$, and $u_{i,s}$ denote group velocities of the signal (idler) photons in the medium; while the second-order correlation function is calculated to be

$$G^{(2)}(\tau) \sim \left| \int_{-\infty}^{\infty} d\Omega F(\Omega) e^{i(k''_s z_s + k''_i z_i) \Omega^2 / 2} \cos(\Omega \tau) \right|^2, \quad (6)$$

where $\tau \equiv [t_2 - (z_i/u_i + r_2/c)] - [t_1 - (z_s/u_s + r_1/c)]$ and we have considered second-order dispersion derivatives k''_s, k''_i for the signal and idler, respectively. In the case of CW pumping, $G^{(2)}$ depends only on τ . One can notice immediately that the shapes of $G^{(1)}$ and $G^{(2)}$ can be quite different, although both of them are associated with the spectral amplitude. It is clear to see that $G^{(2)}$ gets broadened in a transparent dispersive medium while $G^{(1)}$ remains unbroadened. The form of the spectral amplitude $F(\Omega)$ for SPDC is well-known [5]. For type-II SPDC (and for type-I non-degenerate SPDC),

$$F_{II}(\Omega) = \frac{\sin(DL\Omega/2)}{DL\Omega/2}, \quad (7)$$

where L is the crystal length and D is the inverse group velocity difference for signal and idler photons. In the case of type-I frequency-degenerate SPDC, the shape is

$$F_I(\Omega) = \frac{\sin(D''L\Omega^2/2)}{D''L\Omega^2/2}, \quad (8)$$

with D'' denoting the second derivative of the dispersion dependence $k(\omega)$ in the nonlinear medium for signal and idler photons. The corresponding shapes of the two-photon amplitude $F(\tau)$ can be obtained from the Fourier transforms of Eqs. (7) and (8). The typical natural width of $G^{(2)}$ for SPDC (without group-velocity broadening) is in the order of hundreds of femtoseconds, which is impossible to measure directly due to the relatively low time resolution of the existing photon counting detectors. It might seem that the $G^{(2)}$ shape could be measured by means of the “anti-correlation” effect [7] [8] [9] (or other two-photon interference effect), which is based on measuring coincidence counting rate. However, one can show that the shape of the “anti-correlation” “dip” is given not by $G^{(2)}$ but by $G^{(1)}$ [10]. The situation is very similar to that of the classical case: one has to use an “auto-correlator” to

measure the group-velocity broadening of a laser pulse, instead of an interferometer. Unlike the first-order correlation function and the spectrum, the unbroadened second-order correlation function for SPDC radiation is so far impossible to observe even by using the current state-of-the-art photon counting detectors. However, after the group-velocity broadening, for example propagating along a dispersive optical fibre of certain length, it may be broadened enough to be measurable. In the present paper, we demonstrate experimentally how to monitor the broadened $G^{(2)}$ by using the TAC-MCA system, which is quite useful and important in certain types of two-photon correlation measurements.

Consider the propagation of two-photon light through a dispersive transparent medium. The spectrum of SPDC and hence, the first-order correlation function do not change. However, the second order correlation function $G^{(2)}$ does change in this case. The situation is analogous to the propagation of short classical laser pulses through a group-velocity dispersive medium [11]: although the spectrum of a pulse does not change, its shape changes, being broadened. In the far-field zone, i.e., at $z \gg z_{dis}$, where the dispersion length $z_{dis} = \tau_0^2/2\pi k''$ and τ_0 is the initial pulse length, the pulse length varies as $\tau = \tau_0 z/z_{dis}$, and the pulse takes the shape of the initial spectrum. A surprising fact in the case of the entangled two-photon light is that there are no “pulses”, either broadened or unbroadened, associated with either signal or idler photons; it is the biphoton and the second-order correlation function that behave like a “pulse”, which is broadened in the dispersive medium! In the far-field zone, the shape of the second-order correlation function $G^{(2)}$ is

$$G^{(2)}(\tau, z) \sim |F(\Omega)|^2|_{\Omega=\tau/(k'_i z_i + k'_s z_s)}, \quad (9)$$

i.e., has the same shape as the spectrum of the SPDC. To demonstrate this behavior experimentally, we used the setup shown in Fig. 1. A BBO crystal (we used both type-I and type-II samples cut for degenerate collinear phase matching) was pumped by an Ar laser at wavelength $457.9nm$. After passing the SPDC crystal, the pump radiation was cut by a mirror with high reflection at the pump wavelength and high transmission at the signal - idler wavelength. For further blocking of the noise, RG715 color glass filter was placed

behind the mirror. The angular selection of the signal-idler radiation was done by a 2mm pinhole placed at a distance of 1.5m from the crystal. After passing the aperture, the signal and idler radiation was fed into a single-mode polarization-maintaining fibre of length 2m or 500m , for different experimental demonstration. The slow and fast axes of the fibre were aligned according to the polarization directions of the ordinary and extraordinary rays in the BBO crystal. After the fibre, the output beam was split by a polarizing beamsplitter and sent to two single-photon counting modules (Perkin&Elmer SPCM-AQR-14). In the case of type-II BBO, the PBS separated signal and idler photons. In the case of type-I, a half-wave plate after the fibre was used to rotate the polarization by 45° ; this way, the output part of the setup worked as a Hanbury Brown-Twiss interferometer with a 50% beamsplitter. For a better blocking of the noise, color glass filters RG830 were inserted in front of the detectors. The photocurrent pulses from the first and second detectors were sent, respectively, to the “start” and “stop” inputs of a TAC. Since the counting rate of the detectors did not exceed 10^5 counts per second, the distribution at the MCA output corresponded to the $G^{(2)}(\tau)$ function [12]. To find the time resolution of the setup, we first measured the MCA distribution for the case of 5mm type-II BBO crystal without the use of optical fibre (Fig. 2) [13]. According to this measurement, the resolution of the setup is found to be 700ps . For a 3mm type-II BBO, passing the signal and idler radiation through a 500m optical fibre does not spread much the observed MCA distribution. Indeed, the width increase of the second-order correlation function after the fiber should be 50ps in this case, which is much less than the resolution. However, for a 400μ type-II BBO, the initial $G^{(2)}$ is a rectangle with the width of 60fs . The calculated value of z_{dis} is in this case 1.8cm . After the fibre, the width of the $G^{(2)}$ should be about 3ns , which is measurable by means of our TAC-MCA setup. The resulting distribution is plotted in Fig. 3. The shape of the $G^{(2)}$ becomes similar to the initial spectrum of type-II SPDC shown in Eq.(6), with distinct side lobes. The solid line in the plot is a fit using Eq.(6), the only fitting parameter being k'' for the fibre. The parameter D was calculated from the Selmeier equations for BBO; for wavelength 916nm and cutting angle 36.6° of collinear degenerate phase matching, $D = 1.5(\text{ps}/\text{cm})$. For k'' of the fibre, we

obtained a value of $3.2 \cdot 10^{-28} (s^2/cm)$, which is very close to the values typically observed for single-mode fibres (see, for instance, [14]). The SPDC spectrum for $3.4mm$ type-I BBO is broader than the spectrum for $0.4mm$ type-II crystal. Correspondingly, the $G^{(2)}$ broadening by a $500m$ fibre (Fig. 4) is even greater than that for Fig. 3. The shape resembles the spectrum for type-I SPDC. The theoretical calculation (solid line) was done with the same value of k'' as shown in Fig. 3. As D'' , we took the figure $D'' = 5.9 \cdot 10^{-28} (s^2/cm)$, which is calculated from the results of $G^{(1)}$ measurement in type-I BBO [15].

Consider now what happens if narrow-band filters are inserted in front of the detectors D_1 and D_2 . In this case, the filters would cut the central part of the SPDC spectrum. The effect is the same as if $F(\Omega)$ were narrowed or the initial $G^{(2)}(\tau)$ were broadened. Hence, the insertion of filters would reduce the broadening effect of the fibre. In agreement with this, we observed almost no spreading for a 500 m optical fiber if 10 nm interference spectral filters were inserted in front of D_1 and D_2 , see Fig. 5.

Finally, two important conclusions should be formulated.

1. Although both first-order and second-order correlation properties of two-photon light generated via SPDC are initially determined by the spectral amplitude function, they behave differently after the propagation in a dispersive medium. It is necessary to find an effective method of monitoring the broadening of the second-order correlation function $G^{(2)}(\tau)$ for certain two-photon entanglement applications.

2. Passing a biphoton through a dispersive medium one can affect the shape of the biphoton wavepacket. To be precise, one can at least spread the second order correlation function as we have shown. To our belief, the reverse process of compressing the width of the two-photon wavepacket is also possible, of course only within the reach of a Fourier-transform limit. A dispersive medium with the reverse coefficient may be applied in this case [16]. A special type of optical fibre, diffraction grating or a prism pair can be used for this purpose. The situation is almost identical to the manipulation of the shape of a short laser pulse [17]; however, it is the manipulation of the biphoton wavepacket but not the signal or the idler. This effect is of high importance for the applications of two-photon

and multi-photon states in quantum communication and quantum information processing.

We are grateful to M.Rubin for illuminating discussions. This work was supported in part by NSF, ONR and NRO. MVC and AST also acknowledge support from INTAS 01-2122.

*Permanent address: Dept. of Physics, Moscow State University, Moscow, Russia.

†Permanent address: MagiQ Technologies Inc., 11 Ward St. Suite 300, Somerville, MA 02143. Also affiliated with A.F. Ioffe Physical Technical Institute RAS, 26 Polytekhnicheskaja, 194021 St. Petersburg, RUSSIA

REFERENCES

- [1] D.N. Klyshko, A.N. Penin, Sov. Physics-Uspekhi, **30**, 716 (1987).
- [2] A. Ekert, D. Bouwmeester, A. Zeilinger, *The Physics of Quantum Information* (Springer, 2000).
- [3] A. Boto, P. Kok, D. Abrams, S. Braunstein, C. Williams, and J. Dowling, Phys. Rev. Lett., **85**, 2733 (2000); M.D'Angelo, M.V.Chekhova, and Y.H. Shih, Phys. Rev. Lett., **87**, 013602(2001).
- [4] R.J. Glauber, Phys. Rev. **130**, 2529 (1963); **131**, 2766 (1963).
- [5] D.N. Klyshko, *Photons and Nonlinear Optics* (Gordon & Breach, New York,1988).
- [6] M.H. Rubin, D.N. Klyshko, and Y.H. Shih, Phys. Rev. A **50**, 5122 (1994).
- [7] C.K. Hong, Z.Y. Ou, and L. Mandel, Phys. Rev. Lett., **59**, 2044 (1987).
- [8] Y.H. Shih and C.O. Alley, Phys. Rev. Lett., **61**, 2921 (1988).
- [9] A.M. Steinberg, P.G. Kwiat, and R.Y. Chiao, Phys. Rev. Lett., **68**,2421 (1992).
- [10] A.V. Burlakov, M.V. Chekhova, O.A. Karabutova, and S.P.Kulik, Phys. Rev. A, **64**, 041803(R) (2001).
- [11] S.A. Akhmanov, S.Y. Nikitin, *Physical Optics* (Clarendon Press, 1997).
- [12] L. Mandel and E. Wolf, *Optical Coherence and Quantum Optics*(Cambridge University Press, 1995).
- [13] For better accuracy, most of MCA distributions were averaged over 10 channels.
- [14] J.K. Ranka, R.S. Windeler, and A.J. Stentz, Optics Lett., **25**,25 (2000).
- [15] M.V. Chekhova, S.P. Kulik, and Y.H. Shih, to be published.
- [16] J.D. Franson, Phys. Rev. A, **45**, 3126 (1992).

- [17] W. Rudolph, B. Wilhelmi, *Light Pulse Compression, in: Laser Science and Technology. An international handbook.* (Harwood Academic Publishers, 1989).

FIGURES

FIG. 1. The experimental setup.

FIG. 2. The MCA distribution for the case of a $5mm$ type-II BBO crystal and no fibre. The distribution is basically determined by the time resolution of the detectors.

FIG. 3. The MCA distribution for the case of an $0.4mm$ type-II BBO crystal and a $500m$ fibre. The shape is similar to the spectrum for type-II SPDC.

FIG. 4. The MCA distribution for the case of a $3.4mm$ type-I BBO crystal and a $500m$ fibre. The shape is similar to the spectrum of type-I SPDC.

FIG. 5. The MCA distribution for the case of $0.4mm$ type-II BBO crystal, 500 m fibre, and $10nm$ filters inserted in front of the detectors. As a result, the $G^{(2)}(\tau)$ function is not spread, and the width of the distribution remains the same as for the case of a short fibre.

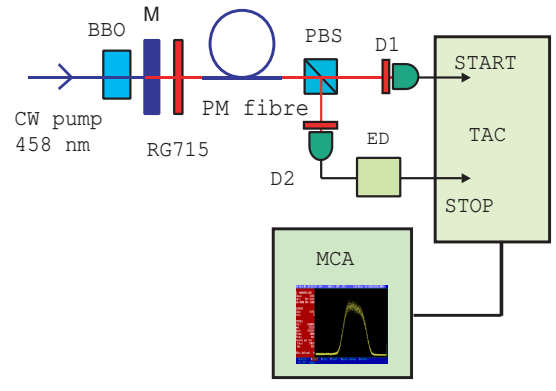


Figure 1. Alejandra Valencia, Maria V. Chekhova, Alexei Trifonov, and Yanhua Shih.

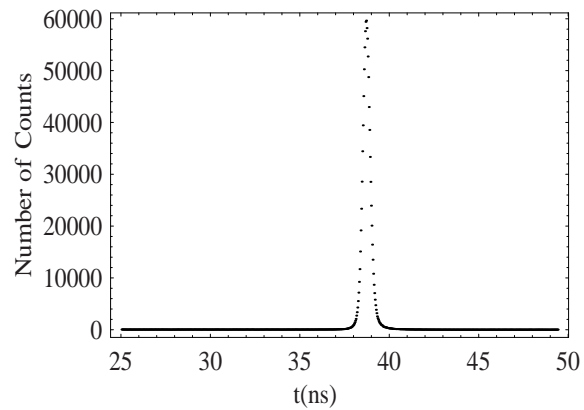


Figure 2. Alejandra Valencia, Maria V. Chekhova, Alexei Trifonov, and Yanhua Shih.

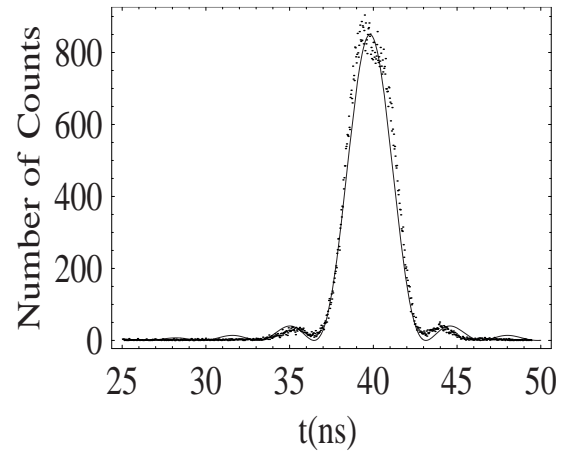


Figure 3. Alejandra Valencia, Maria V. Chekhova, Alexei Trifonov, and Yanhua Shih.

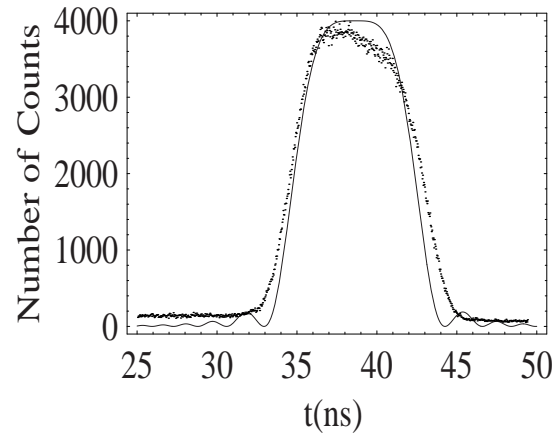


Figure 4. Alejandra Valencia, Maria V. Chekhova, Alexei Trifonov, and Yanhua Shih.

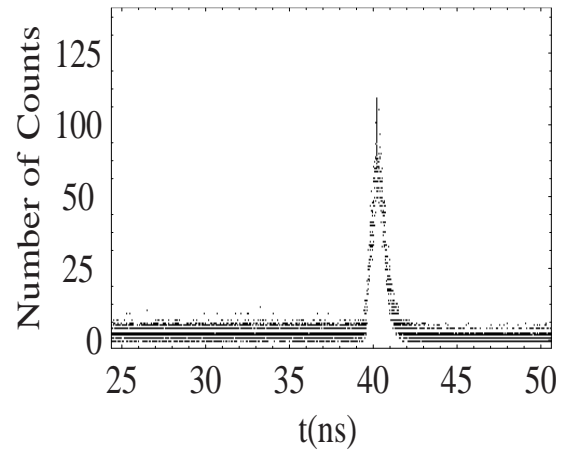


Figure 5. Alejandra Valencia, Maria V. Chekhova, Alexei Trifonov, and Yanhua Shih.